Radiation belt representation of the energetic electron environment: Model and data synthesis using the Salammbô radiation belt transport code and Los Alamos geosynchronous and GPS energetic particle data

S. Bourdarie,[1] R. H. W. Friedel,[2] J. Fennell,[3] S. Kanekal,[4,5] and T. E. Cayton[2]

Received 28 January 2004; revised 4 August 2004; accepted 10 December 2004; published 13 April 2005.

[1] The highly energetic electron environment in the inner magnetosphere (geosynchronous Earth orbit (GEO) inward) has received a lot of research attention in resent years, as the dynamics of relativistic electron acceleration and transport are not yet fully understood. These electrons can cause deep dielectric charging in any space hardware in the medium Earth orbit (MEO) to GEO region. We use a new and novel approach to obtain a global representation of the inner magnetospheric energetic electron environment, which can reproduce the absolute environment (flux) for any spacecraft orbit in that region to within a factor of 2 for the energy range of 100 KeV to 5 MeV electrons for any level of magnetospheric activity. We combine the extensive set of inner magnetospheric energetic electron observations available at Los Alamos with the physics-based Salammbô transport code using the data assimilation technique of ''direct-insertion.'' This, in effect, inputs in situ data into the code and allows the diffusion mechanisms in the code to interpolate the data into regions and times of no data availability. Here we present details of the methods used both in the data assimilation process and in the necessary intercalibration of the input data used. We present sample runs of the model/data code and compare the results to test spacecraft data not used in the data assimilation process.

Citation: Bourdarie, S., R. H. W. Friedel, J. Fennell, S. Kanekal, and T. E. Cayton (2005), Radiation belt representation of the energetic electron environment: Model and data synthesis using the Salammbô radiation belt transport code and Los Alamos geosynchronous and GPS energetic particle data, *Space Weather*, *3*, S04S01, doi:10.1029/2004SW000065.

1. Introduction

[2] The natural energetic electron environment in the Earth's radiation belts is of general importance as dynamic variations in this environment can impact space hardware and contribute significantly to background signals in a range of other instruments flown in that region.

[3] There is intense interest in isolating and understanding the mechanisms that contribute to the MeV electron flux buildups in the inner magnetosphere which are frequently observed during the recovery phase of geomagnetic storms. While this is not a new topic, the unprecedented density of observations of relativistic electrons in the inner magnetosphere in the modern era has led to new questions and unsolved problems. In a recent review, *Friedel et al.* [2002] covers in detail the current state of research into this topic.

[4] The interest in these events arises in part because of the increasing evidence of the correlation between the occurrence of relativistic electron flux enhancements and of subsequent spacecraft operating anomalies or failures, especially at geosynchronous altitude. The prediction and mitigation of these effects should be possible when the causes of the flux buildups are understood [*Baker*, 1996]. In addition, because of the apparent complexity of these mechanisms, their understanding will contribute significantly to the general knowledge of transport, heating and loss processes in the magnetosphere.

[5] The scientific community is engaged in understanding the underlying physics to the observed dynamics, and being able to put one's data into the context of a global model is a necessary step; however, the question that is of most importance to spacecraft operators that are faced with an anomaly on a spacecraft is: ''Was my anomaly due to the environment?'' To answer this question one needs to be able to accurately describe the environment at any point in the inner region, even in the absence of in situ measurements.

[6] Data from any single point measurement in space have traditionally been used to derive information about the local environment at that satellite. There have been some earlier attempts of obtaining a dynamic global state of the inner magnetospheric electron populations based on

[1]Office National d'Etudes et de Recherches Aerospatiales/Departement Environnement Spatial (ONERA/DESP), Toulouse, France.
[2]Los Alamos National Laboratory, Los Alamos, New Mexico, USA.
[3]The Aerospace Corporation, El Segundo, California, USA.
[4]Department of Physics, University of Maryland, College Park, Maryland, USA.
[5]Now at NOAA Space Environment Center, Laboratory for Atmospheric and Space Physics, University of Colorado, Boulder, Colorado, USA.

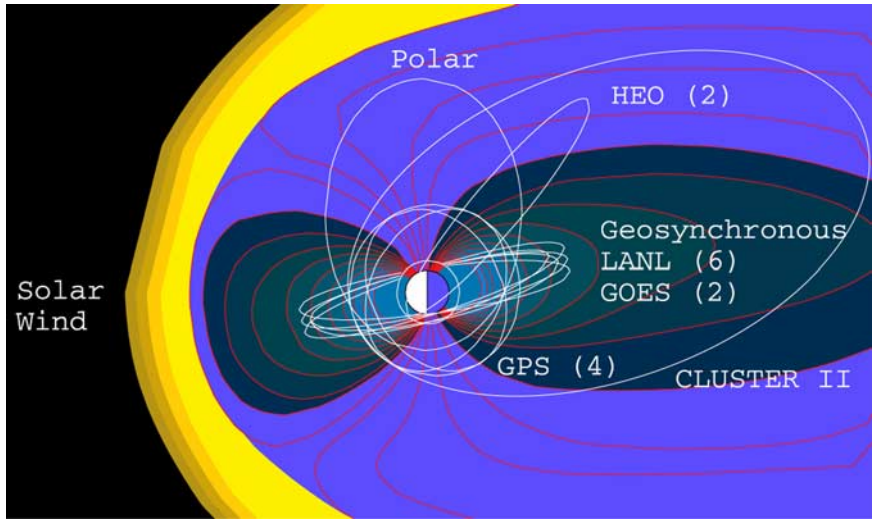

Figure 1. Schematic of current inner magnetosphere missions.

single spacecraft observations, based on the CRRES data, our community's last mission dedicated to the radiation belts. CRRES alone, on a 5.5-hour resolution, was able to provide a basically complete description of the inner region, across a wide energy range, owing to its ideally suited geosynchronous transfer orbit [*Friedel and Korth*, 1995]. However, CRRES flew in 1990/1991, and one has to look to other resources for such information today.

[7] *Friedel et al.* [2000] used a multispacecraft synthesis using simple interpolation technique with data from up to 11 spacecraft to assemble a ''map'' of the inner radiation belt energetic electron population. This simple approach led to radiation belt maps that could represent the dynamics of the inner region on around a 3-hour timescale, but the simplistic interpolation and intercalibration scheme employed led to many unrealistic local time and radial variations which were clearly not physical, but rather a reflection of insufficient instrument characterization and intercalibration.

[8] In order to characterize this environment, energetic particle detectors have routinely been flow on a range of DOE, NOAA and DOD spacecraft in geosynchronous, GPS and Molniya orbits. Beyond these programmatic missions, this region has also been the subject of purely scientific investigations with current missions such as Cluster (ESA) and Polar (NASA). A schematic of the orbits of these missions available today is shown in Figure 1.

[9] While the scientific measurements can provide the full three-dimensional particle distribution function and local magnetic field data (allowing data to be determined at constant adiabatic invariants, which are the coordinates that allow data to be intercompared throughout the inner magnetosphere), these data are not available on long timescales or on a reliable basis into the future, and, when present, have a limited spatial coverage by themselves. Data from the programmatic missions provide excellent time coverage, longevity and spatial coverage, but with particle instrumentation that provides mainly omnidirectional data and no magnetic field information. The GOES mission does have magnetometers, but limited spectral and spatial resolution.

[10] The challenge is thus to utilize the available data in a framework that still allows us to retrieve high-fidelity global maps of the inner radiation belts. Our approach here is a synthesis between multiple point space measurements and a physics-based radiation belt model that makes full use of all the data from our current constellation of energetic electron measurements in space (up to 6 simultaneous geosynchronous and 4 simultaneous GPS orbit measurements) and uses the model to provide a physical interpolation between the data. The end result is a dynamic and global model of the energetic electron radiation environment at all points in space, which can provide reliable environmental data for locations of satellites that do not carry any energetic particle instrumentation.

[11] Data for our assimilation at this point come primarily from the LANL Geosynchronous SOPA instrument [*Reeves et al.*, 1997] and the LANL GPS energetic particle sensors [*Feldman et al.*, 1985]. For testing purposes we also use data from the HEO energetic particle instruments [*Blake et al.*, 1997].

2. Model

[12] We use here a custom version of the Salammbô radiation belt code developed at ONERA in Toulouse, France [*Beutier and Boscher*, 1995; *Bourdarie et al.*, 1996b; *Boscher et al.*, 2000]. This is a diffusion code that models physical processes in the inner magnetosphere by their respective diffusion coefficients (radial and pitch angle diffusion). A schematic of this code is shown in Figure 2. Radial diffusion is due to a fluctuation spectrum of the magnetic and electric fields, and wave-particle interactions give rise to pitch angle diffusion. Traditionally, the LANL geosynchronous data were used as a boundary condition.

[13] This code uses the planetary disturbance index Kp to parameterize radial diffusion and the position of the

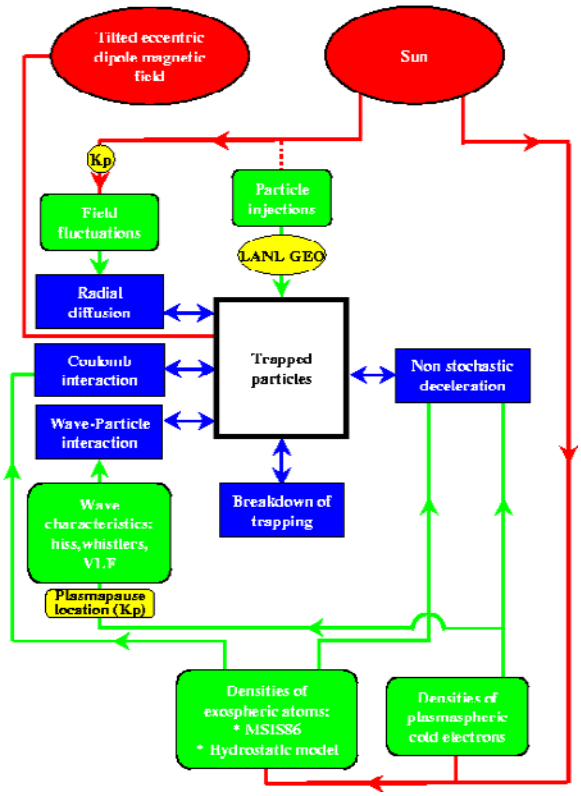

Figure 2. Schematic the Salammbô radiation belt code for electrons.

plasmapause which controls wave activity and thus pitch angle diffusion. The code is symmetrical in local time since on a given drift orbit particle fluxes are the same at all local times on timescales on the order of the drift time, which is typically around 10 min for the highly energetic electrons. The code traces the full particle distribution function in the coordinate space of L* (magnetic coordinate of the drift shell), B/B_{EQ} (the ratio of the local magnetic field strength to the equatorial magnetic field strength on a given magnetic field line) pitch angle and energy.

[14] The code has successfully been used to model the response of the inner magnetospheric energetic electron population to geomagnetic storms [*Bourdarie et al.*, 1996a]. Recent work by *Summers et al.* [1998] pointed out the importance of energy diffusion by whistler mode waves for relativistic electrons as being an important energization source, and *Meredith et al.* [2002] have shown a direct relationship between relativistic electron acceleration and substorm-enhanced whistler mode chorus. This physics is currently not included in the Salammbô code, but, as it turns out, our data assimilation can compensate for this: inclusion of relevant amounts of data "pulls" the code in the right direction, even in the absence of this physical process.

3. Data Preparation

[15] In response to the lessons learned by *Friedel et al.* [2000] a large amount of effort was devoted processing our data to a level that made inclusion into a model feasible. Models in general have no way of distinguishing between "good" and "bad" data; garbage in simply leads to garbage out. Early assimilation runs suffered from stability problems arising from importing data that were wildly different from the model representation. It was necessary to interpolate and clean up the data to a high degree of fidelity before any import of the data into the model was attempted. This effort alone took almost 2 years. Here we present a brief outline of the procedures adopted.

3.1. Intercalibration

[16] It was decided to baseline our data to the last high-fidelity energetic particle instrument flown in the inner magnetosphere, the MEA instrument on board CRRES [*Vampola et al.*, 1992]. This was a magnetic spectrometer with full anticoincidence electronics, that does not suffer some of the background and noise problem encountered on the LANL GEO, GPS and HEO instruments. A high energy extension of the MEA instrument was provided by the HEEF instrument on CRRES which has been carefully intercalibrated with MEA to provide a continuous spectrum to 8 MeV [*Dichter et al.*, 1993]. Using the overlapping time periods between CRRES and LANL GEO and GPS missions, we could intercalibrate those missions to agree with the CRRES measurements. This requires the definition of conjunctions between two spacecraft. In order to obtain a sufficient number of conjunctions, we used the following set of conditions: (1) $L < 6$ and $\Delta L < 0.1$; (2) $\Delta B/B_{EQ} < 0.1$ (close to the magnetic equator); (3) magnetic local time (MLT) within 2 hours of 0600 and 1800 and $\Delta MLT < 0.15$ (see Figure 3); (4) magnetospheric activity quiet ($Kp < 2$ for two days before conjunction; and (5) $\Delta t < 3$ hours.

[17] The restriction in local time is due to the use of model magnetic fields in obtaining the required model coordinates (L*), which are best in these regions. The low activity requirement allows us to relax the time constraint on conjunctions; this allows us to obtain more conjunction points. Finally, since GEO and GPS can never fulfill the conjunction requirements used here, they were both independently calibrated against CRRES, which has conjunctions with both.

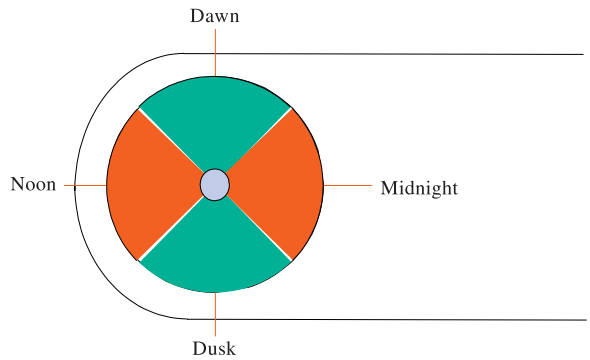

Figure 3. Schematic showing the green region of "allowed" conjunctions.

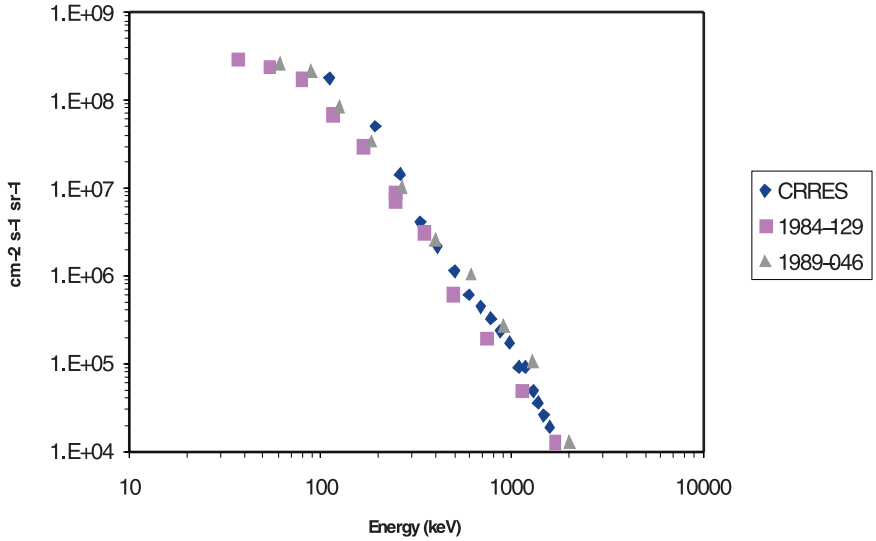

Figure 4. Matching spectra between CRRES and two LANL GEO spacecraft in September 1990.

[18] Figure 4 shows our resulting intercalibration between LANL geosynchronous and CRRES data, showing an excellent match.

[19] Figure 5 shows the result of intercalibrating CRRES with GPS ns18. For the GPS spacecraft, the energy thresholds are gain dependent; the red triangles show the raw, uncorrected data and the black crosses the new spectra after adjusting the energy thresholds to match the CRRES spectra.

[20] Once these calibrations had been done the calibrations were propagated forward in time. This was done by forming long-time averages of overlapping GPS and GEO data and introducing correction factors for each energy channel to match the "older" data set. For GPS this was done by comparing the data over the same L value ranges. An additional complication for GPS was that the instruments gain settings were periodically adjusted which changed both the efficiency and energy thresholds of the measured channels. Time-dependent drift for these gain factors provides another challenge and the intercalibration was only possible due to the fact that overlapping time periods were sufficiently long and that we never had just one GPS spacecraft at a given time.

[21] In this way a consistent set of intercalibration data for all GPS and GEO spacecraft could be established to the present. Our best estimate of the accuracy of this intercalibration is that on average the calibration is good to within a factor of 2; this is based on the fact that between any two spacecraft the calibrations agreed to within a factor of two over the time period of joint measurements. However, it must be pointed out that a rigorous error analysis and error propagation has not yet been performed. The details

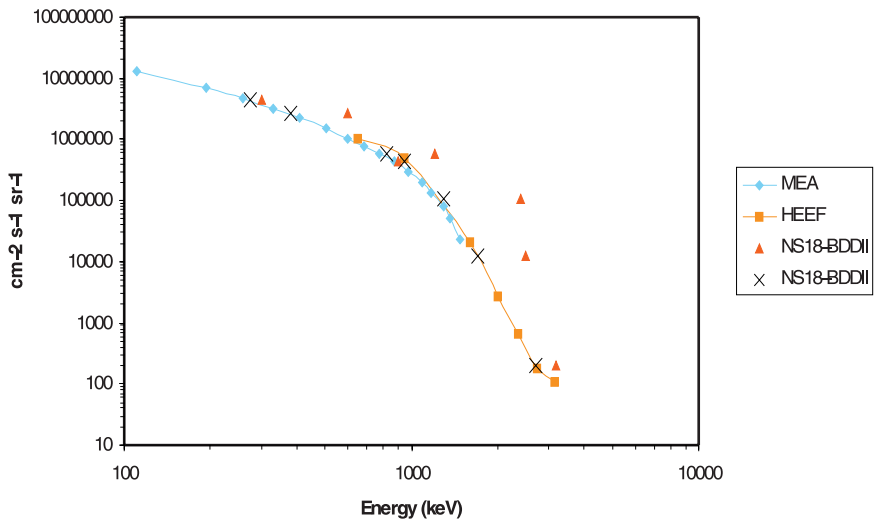

Figure 5. Matching spectra between CRRES and GPS ns18 spacecraft in September 1991.

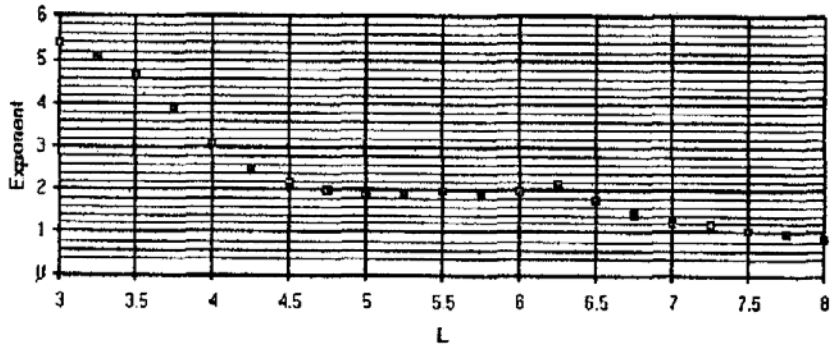

Figure 6. CRRES mission averaged pitch angle distribution coefficient s for 510 keV electrons as a function of L. From [*Vampola*, 1997].

of this calibration procedure are somewhat complex and instrument specific and can be found in a 60-page document available at http://nis-www.lanl.gov/~friedel/lws_proj/GPS_calibration_2002.doc.

3.2. Data Contamination

[22] It is well known that during times of solar energetic proton events (SEPs) many of the detectors used here are contaminated with strong background counts. We use the NOAA GOES energetic proton data to mask out our data during such active times, by monitoring a threshold flux of 10^{-5} (cm^{-1} s^{-1} sr^{-1} keV^{-1}) on the 39–82 MeV proton channel. During times when this threshold is exceeded we do not assimilate any data into our model but allow the model to run freely.

3.3. Saturation/Background

[23] Data saturation occurs in some instruments as a limit of counting speed during high count intervals, leading to an artificial plateau in observed counts. These levels are statistically observable and we can ensure that only those data below saturation levels are used in the assimilation process.

[24] Background levels due to thermal noise or other contamination such as cosmic rays are present in all particle instruments. These levels can be detected by examining data during intervals when the spacecraft are outside the trapping region for energetic electrons, this occurs over the polar cap on open field lines for GPS and during extreme magnetospheric compression events for the geosynchronous regions. We detect and track these background counts over time and subtract these counts before using the data in our assimilation.

4. Data Assimilation Techniques

[25] This model has been tightly integrated into our data systems at ONERA and LANL, and allows us to input data from various spacecraft sources directly into the model grid. The difference here is that the model no longer uses a simple boundary condition, but allows direct input into the code grid at any location for which data are available. This corresponds to the data assimilation method of direct insertion, which can be thought of the simplest form of "nudging" [*Ghil and Malanotte-Rizzoli*, 1991].

4.1. Data Input

[26] In order to seed the code with real data, the data have to be transformed into the model coordinate space. The Salammbô code internally uses a custom spaced grid in energy, pitch angle and L* (Roederer-L). L* here corresponds to the third adiabaticin variant and is closely related to a particle's drift shell. For energetic particles for which electric field drifts can be ignored, L* almost exactly labels the drift shell a real particle follows. In contrast, the traditional L (McIlwain L) labels a single field line only.

[27] Owing to the nature and limitations of the data used the determination of this mapping requires some assumptions:

[28] 1. L* depends on a magnetic field model. At this stage of our assimilation work we use the same model for all data, the static Olson Pfizer 1977 model. This is certain to introduce inaccuracies in the mapping of the data into the model during active times, and we consider this a first step which at least puts all the data into the same coordinate system. Extensions to more complex and dynamic models are planned.

[29] 2. Current data sources provide omnidirectional data and no magnetic field information. We thus use a statistical representation of pitch angle distributions (such as $j \sim \sin^{2s} \alpha$) as a function of L*. Figure 6 shows results for s from the CRRES spacecraft [*Vampola*, 1997]. This is overwritten at times when we are able to determine the pitch angle distribution directly from data (see Figure 7). Whenever there are "conjunctions" in the input data (satellites at the same L* but at different magnetic latitudes) we use a fitting procedure to derive the best fit to a pitch angle distribution that yields the observed omnidirection data at the two latitudes. Using a pitch angle distribution of the form $j \sim \sin^{2s} \alpha$ at the equator, the omnidirectional flux at the satellite can be represented by

$$J_{OMNI} = 4\pi \int_0^{\alpha(I90_{EQ})} j \sin^n \alpha \sin \alpha d\alpha$$

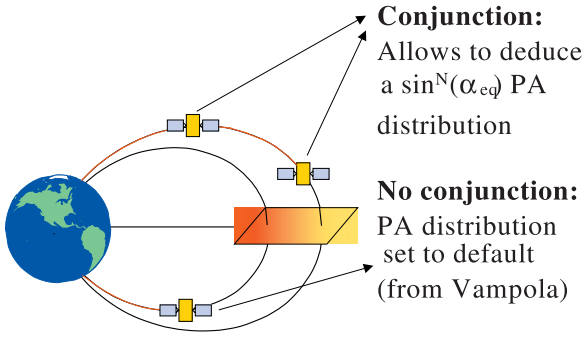

Figure 7. Schematic of model "conjunctions" allowing determination of pitch angle distribution from omnidirectional data.

where $\alpha(l90_{EQ})$ is the equatorial pitch angle of the particles just mirroring at the satellite. Given two measures of J_{OMNI} we can solve for n and j; for more than 2 measures, we use a least squares fit. This n is strictly only valid for particles with mirror points above the satellite's latitude, so we assign all pitch angles from the lowest B/B_{EQ} to the loss cone to the fit. Such "measured" pitch angle distributions override the statistical distributions with a persistence of 1 hour.

[30] 3. Energy channels are interpolated to the required grid energy values. Measurements are assigned to the two closest grid points in L weighted according to their distance from the grid point, to ensure smooth data insertion. Given the value at grid point a, f_a the value at grid point b, F_b, the total distance between the grid points, d, the inserted data value f_i, and its distance to grid points a and b, d_a and d_b respectively, the "new" values at grid points a and b are assigned thus:

$$f_a(new) = f_a + d_a/d * abs(f_a - f_i)$$

$$f_b(new) = f_b + d_b/d * abs(f_b - f_i)$$

[31] 4. The outer boundary of the simulation is at L* = 9. The value of this boundary is either set equal to the AE8 model value at L = 9 [*Vette*, 1991], or when GEO data are available to the geosynchronous data values adiabatically shifted to L* = 9. This involves taking the geosynchronous spectrum in the model and the model dipole field to preserve the first adiabatic invariant, to find the spectrum at L* = 9. This in effect assumes adiabatic radial transport from L* = 9 to geosynchronous orbit.

[32] We need to point out that the methods described here represent our first approach and are constantly being refined. As the model evolves (finer grid spacing) and our data evolve (inclusion of pitch angle sorted data from LANL GEO, POLAR and CLUSTER) our assimilation techniques will become more complex. In a general run input data thus transformed are entered into the grid for the locations and times available, and the model is allowed to act for all other periods and locations.

4.2. Model Output

[33] The output of the Salammbô code is a time series of states in model coordinates that define the global inner radiation belt for energetic electrons in L* (1.1 to 9). The time resolution currently is 10 s.

[34] Once a model run for a given set of input data for a given period has been performed, we can "fly" any required spacecraft orbit through the model grid. All we need to do is to transform any satellite ephemeris to the required magnetic coordinates of the model grid and specify which energy we want. The model can return data either in differential or integral energy flux, either pitch angle resolved or summed to give an omnidirectional equivalent.

5. First Results

[35] An initial run was performed for the period of the NSF GEM storm of 1 September to 10 October 1998. The model was run with the correct Kp values for this period, and data were assimilated into the model from one geosynchronous satellite (LANL-GEO 1994_084) and one GPS satellite (ns33). The model output at one time step is shown in Figure 8. In order to assess model performance we used several test satellites that were "flown" through the model results. We then compared the model fluxes versus the actually measured fluxes on the test satellites.

5.1. Model and LANL GEO and HEO Data As a Test

[36] Here we performed our model run using only the LANL GEO data as input. The results are shown in Figure 9. The model is initialized with a default state at the beginning of the run representing an average quiet magnetosphere, taken from CRRES measurements.

[37] HEO data are used as a test: At this point HEO HAS NOT been fully intercalibrated with GEO and GPS. Initial comparisons, however, show that for the energy range chosen in our comparisons here, agreement between HEO, GPS and GEO is generally good.

[38] The description of Figure 9 also applies to Figures 10 and 11. The top three panels show data in the L* versus time format, where each color coded vertical bar in the plot represents the flux along the satellites cut through L* at this time. The top panel shows the actual HEO-3 satellite data for the >0.63 MeV channel. The next panel shows the model output along the orbit on HEO-3; both these panels share the same color bar. The third panel shows the ratio model divided by data, and the color bar represents ratios up to 10 in yellow/red graduations and ratios down to 0.1 in blue/dark blue graduations. The bottom panel shows the Dst storm index for reference.

[39] Ideally, if model and data agree 100%, this ratio should be 1 (black). Here we see large deviations from 1 in two areas: the outer belts near GEO and the inner region near the slot. The first discrepancy can be explained in terms of the missing model physics as described earlier:

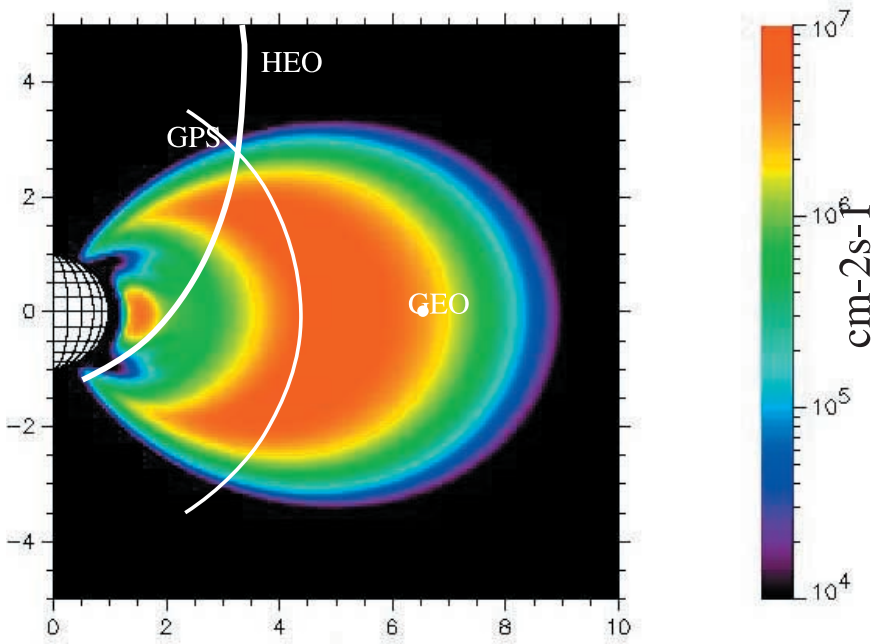

Figure 8. A graphical representation of the model fluxes at one time step in the simulation. Shown superimposed are the orbits of LANL GEO and GPS and HEO (used for testing output only).

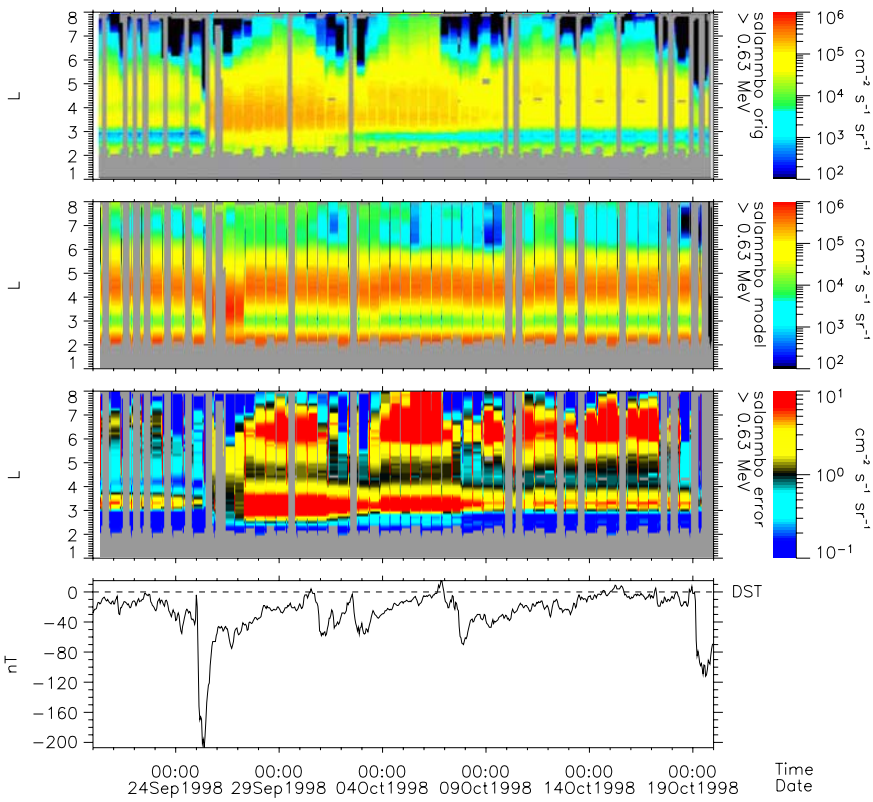

Figure 9. Data, model, and comparison outputs: Model and LANL GEO, HEO as test. See text for details.

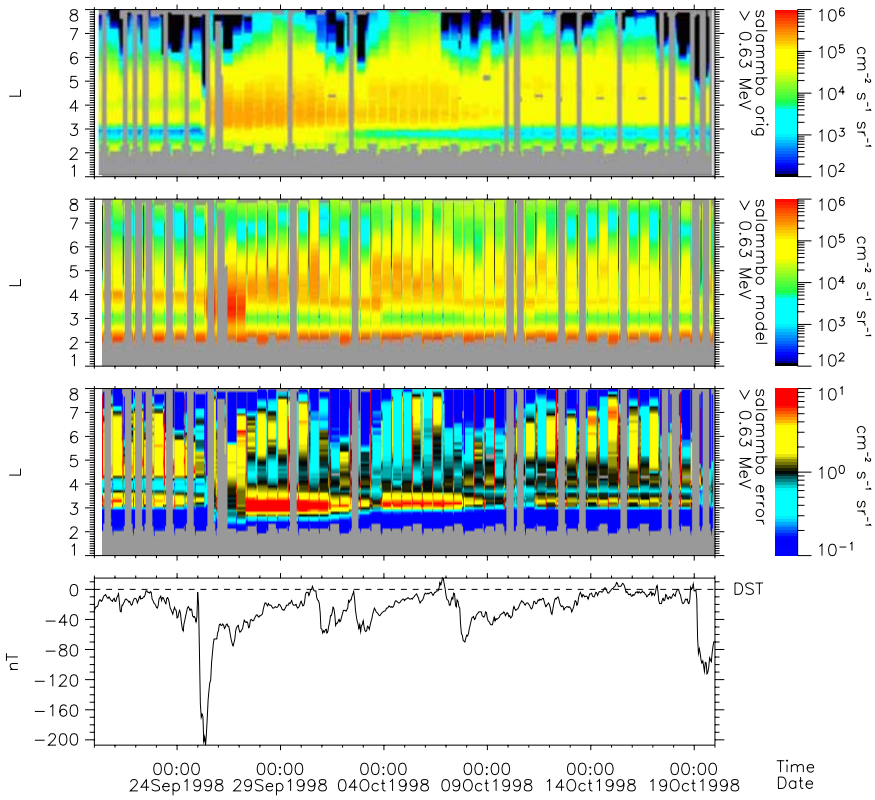

Figure 10. Data, model and comparison outputs: Model and LANL GEO and GPS, HEO as test. See text for details.

whistler chorus interactions are not yet modeled, and in the absence of any assimilation data inside of geosynchronous that helps define the GEO pitch angle distributions. The HEO test spacecraft has a highly elliptical orbit and cuts through GEO at high latitude. The model data here are highly dependent on the assumed pitch angle distribution at the equator, which here comes from a statistical model. We know that energetic electron pitch angle distributions can be highly variable during storms [*Blake et al.*, 2001]. Obviously the statistical pitch angle representation is not a good one for this time period. The discrepancy at low L is simply due to wrong initial state and short model run: diffusion is extremely slow in this region and we simply observe a persistence of the initial state.

5.2. Model and LANL GEO, GPS, and HEO Data As a Test

[40] This model run uses both the LANL GEO and GPS data as input, which assimilates data into the region down to L = 4. The results are shown in Figure 10. As a quick visual comparison between Figures 9 and 10 easily shows the model performance is much improved by the inclusion of just one additional satellite in the assimilation process. This is particularly true for the region which is now covered by data input; GPS data are available from L = 4 outward, and in that region the model/data comparison shown mainly black and light yellow indicating performance of model to within a factor of 2–3 of the data. Inclusion of GPS around L = 4 to 5 compensates for the missing physics in the region, while near GEO it helps to properly define the pitch angle distribution which is needed to correctly estimate the fluxes at the high latitudes of HEO. The inner region remains badly represented here since no additional satellite data were used there. The addition of low-altitude data from SAMPEX will help out in this region.

5.3. Model and LANL, GEO and GPS, Another GPS As Test

[41] This model run uses both the LANL GEO and GPS ns33 data as input, but uses another GPS satellite, ns24 as the test satellite. The results are shown in Figure 11.

[42] Not surprisingly the model data comparison shows consistent ratios of 2–3 throughout the whole period, regardless of activity levels. This is expected as the region tested is also the region seeded with assimilation data. What the residual ratios of 2–3, however, indicate is that this is about as good as we can hope to get with this method. Factors of 2–3 represent the fidelity of our original data intercalibration.

6. Summary

[43] This project is in its initial stages and a lot of further fine tuning of the assimilation method and input data is

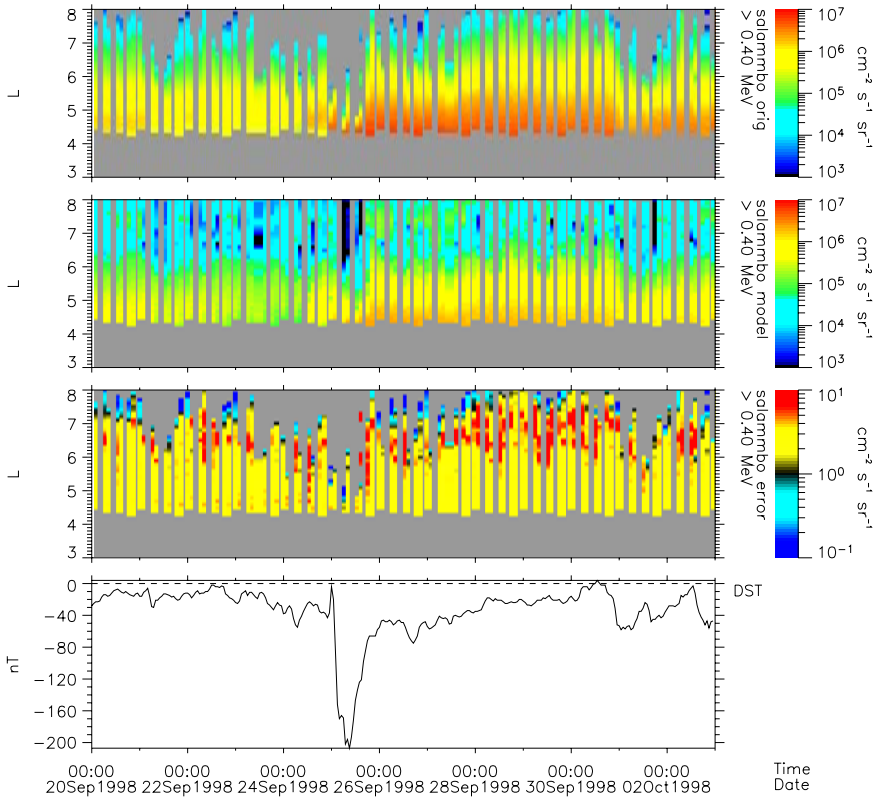

Figure 11. Data, model and comparison outputs: Model and LANL GEO and GPS, another GPS as test See text for details.

needed. First results, however, are promising. We are confident that for spacecraft orbits in the MEO to GEO orbital range we can reproduce the real environment with this method to within factors of 2–3.

[44] We will extend our model further to include as many data sources as possible, especially at lower altitudes. It must be noted that before further data can be incorporated a similar intercalibration effort as done for GEO and GPS needs to be undertaken for HEO, POLAR, SAMPEX and CLUSTER. Further, once pitch angle resolved input data are being used from GEO, POLAR and Cluster our data assimilation methods need to be upgraded to correctly map the data into the model, as shell splitting effects in real magnetic fields need to be taken into account.

[45] We anticipate using this model/data synthesis both for research and for space weather now-casting (limited by real-time data availability, currently not possible for GPS). For research, having this model "specify" the real environment we can then run the model in a nonassimilative mode to see what physics is missing/under-represented. For space weather, we can specify the environment for any past time going back approximately one solar cycle, which is required for any postevent anomaly analysis. Further, we can use this model to explore exactly what kinds of data and data locations are needed for optimal input that would increase the fidelity of the model.

[46] **Acknowledgments.** We thank R. D. Belian, R. A. Christensen, and M. M. Meier for providing assistance with the LANL satellite data and W. Feldman and C. Ingraham for the GPS data. This work was supported by grant W-19,957 from NASA's Living with a Star Research and Technology Program and from the U.S. Department of Energy Office of Basic Energy Science and from ONERA internal funding.

References

Baker, D. N. (1996), Solar wind-magnetosphere drivers of space weather, *J. Atmos. Terr. Phys.*, *58*, 1509–1525.

Beutier, T., and D. Boscher (1995), A three-dimensional analysis of the electron radiation belt by the Salammbô code, *J. Geophys. Res.*, *100*, 14,853–14,861.

Blake, J. B., D. N. Baker, N. Turner, K. W. Ogilvie, and R. P. Lepping (1997), Correlation of changes in the outer-zone relativistic-electron population with upstream solar wind and magnetic field measurements, *Geophys. Res. Lett.*, *24*, 927–929.

Blake, J. B., R. S. Selesnick, D. N. Baker, and S. Kanekal (2001), Studies of relativistic electron injections events in 1997 and 1998, *J. Geophys. Res.*, *106*, 19,157–19,168.

Boscher, D., S. Bourdarie, R. M. Thorne, and B. Abel (2000), Influence of the wave characteristics on the electron radiation belt distribution, *Adv. Space Res.*, *26*(1), 163–166.

Bourdarie, S., D. Boscher, T. Beutier, J. A. Sauvaud, and M. Blanc (1996a), Magnetic storm modeling in the Earth's electron belt by the Salammbô code, *J. Geophys. Res.*, *101*, 27,171–27,176.

Bourdarie, S., D. Bosher, T. Beutier, J. A. Sauvaud, M. Blanc, and R. H. W. Friedel (1996b), A physics based model of the radiation belt flux

at the day timescale, in *Proceedings of the Symposium on Environment Modelling for Space-Based Applications, SP-392*, pp. 159–163, ESA Publ. Div., ESTEC, Noordwijk, Netherlands.

Dichter, B. K., F. A. Hanser, B. Sellers, and J. L. Hunerwadel (1993), High energy electron fluxmeter, *IEEE Trans. Nucl. Sci.*, *40*, 242–245.

Feldman, W., W. Aiello, D. Drake, and M. Herrin (1985), The BDD II: An improved electron dosimeter for the global positioning system, *Tech. Rep. LA-10453-MS*, Los Alamos Natl. Lab., Los Alamos, N. M.

Friedel, R. H. W., and A. Korth (1995), Long-term observations of keV ion and electron variability in the outer radiation belt from CRRES, *Geophys. Res. Lett.*, *22*, 1853–1856.

Friedel, R. H. W., et al. (2000), A multi-spacecraft synthesis of relativistic electrons in the inner magnetosphere using LANL, GOES, GPS, SAMPEX, HEO and POLAR, *Adv. Space Res.*, *26*(1), 93–98.

Friedel, R. H. W., G. D. Reeves, and T. Obara (2002), Relativistic electron dynamics in the inner magnetosphere—A review, *J. Atmos. Terr. Phys.*, *64*, 265–282. (Available at http://nis-www.lanl.gov/~friedel/publications/first_author/rel_elec_rev_accepted_crc.pdf.)

Ghil, M., and P. Malanotte-Rizzoli (1991), Data assimilation in meteorology and oceanography, *Adv. Geophys.*, *33*, 141–266.

Meredith, N. P., R. B. Horne, R. H. A. Iles, R. M. Thorne, D. Heynderickx, and R. R. Anderson (2002), Outer zone relativistic electron acceleration associated with substorm-enhanced whistler mode chorus, *J. Geophys. Res.*, *107*(A7), 1144, doi:10.1029/2001JA900146.

Reeves, G. D., R. D. Belian, T. C. Cayton, M. G. Henderson, R. A. Christensen, P. S. McLachlan, and J. C. Ingraham (1997), Using Los Alamos geosynchronous energetic particle data in support of other missions, in *Satellite-Ground Based Coordination Source Book*, edited by M. M. Lockwood and H. J. Opgenoorth, pp. 263–272, ESA Publ. Div., ESTEC, Noordwijk, Netherlands.

Summers, D., R. M. Thorne, and F. Xiao (1998), Relativistic theory of wave-particle resonant diffusion with application to electron acceleration in the magnetosphere, *J. Geophys. Res.*, *103*, 20,487–20,500.

Vampola, A. L. (1997), Outer zone energetic electron environment update, paper presented at Conference on the High Energy Radiation Background in Space, Inst. of Electr. and Electron. Eng., Snowmass, Colo., 22 July.

Vampola, A. L., J. V. Osborne, and B. M. Johnson (1992), CRRES magnetic electron spectrometer AFGL-701-5A (MEA), *J. Spacecr. Rockets*, *29*, 592–594.

Vette, J. I. (1991), The NASA/National Space Science Data Center Trapped Radiation Environment Model Program (1964–1991), *Tech. Rep. NSSDC/WDC-A-R & 91-26*, NASA Goddard Space Flight Cent., Greenbelt, Md.

S. Bourdarie, ONERA-CERT/DESP, BP 4025, 2, Avenue Edouard Belin F-31055 Toulouse Cedex 4, France. (sebastien.bourdarie@onecert.fr)

T. E. Cayton and R. H. W. Friedel, Los Alamos National Laboratory, P.O. Box 1663, Los Alamos, NM 87545, USA. (tcayton@lanl.gov; rfriedel@lanl.gov)

J. Fennell, The Aerospace Corporation, Mail Stop M2-259, P.O. Box 92957, Los Angeles, CA 90009, USA. (joseph.f.fennell@aero.org)

S. Kanekal, NOAA/SEC, University of Colorado/LASP, 325 Broadway, Boulder, CO 80305, USA.